Chemical Engineering Journal 148 (2009) 517–524

Contents lists available at ScienceDirect

Chemical Engineering Journal

journal homepage: www.elsevier.com/locate/cej

Characterization of mixing in a hollow fiber membrane contactor by the iodide–iodate method: Numerical simulations and experiments

N. Baccar[a,b,c], R. Kieffer[a,b,c], C. Charcosset[a,b,c,*]

[a] Université de Lyon, F-69622 Lyon, France
[b] Université Lyon 1, Villeurbanne, France
[c] LAGEP, UMR 5007, CNRS, CPE, 43 bd du 11 novembre, 69100 Villeurbanne, France

ARTICLE INFO

Article history:
Received 6 October 2008
Received in revised form 11 December 2008
Accepted 14 December 2008

Keywords:
Dushman reaction
Iodide–iodate reaction
Hollow fiber
Membrane contactor
Mixing
Micromixing

ABSTRACT

This paper presents numerical simulations and experimental data on the iodide–iodate reaction in a hollow fiber membrane device. The principle of reactive mixing in a membrane device is the following. Component **A** flows through the inlet of the lumen side and component **B** comes from the membrane pores (shell side). Components **A** and **B** then mix and react inside the lumen side. Experimental measurements of the segregation index were carried out under various experimental conditions and for two different hollow fiber devices. The numerical and experimental segregation indexes, X_S, were found in the range 10^{-2}–10^{-3}, indicating effective mixing. The numerical simulations showed that I_3^- ions were produced mainly in the first part of the lumen side of the hollow fiber. This confirmed our previous results on precipitation which showed that high supersaturation data and experimental fouling were obtained in this part of the hollow fibers.

1. Introduction

Membrane contactors represent an emerging technology in which the membrane is used as a tool for inter-phase mass transfer operations, i.e. (i) liquid–gas phase processes, such as simultaneous extraction and injection of gases in natural water production, membrane distillation for desalination and wastewater treatment, and (ii) liquid–liquid phase processes, such as reactive mixing [1,2]. The principle of reactive mixing in a hollow fiber membrane device is the following. Component **A** flows through the inlet of the lumen side of the hollow fibers and component **B** comes from the membrane pores (shell side). Components **A** and **B** then mix and react inside the lumen side. This process has been used for the preparation of inorganic particles [3–7], polyaluminium chloride particles [8], L-asparagine crystals [9], and polymeric nanoparticles [10]. Despite the increasing number of reported applications, few works investigated theoretically reactive mixing in a hollow fiber membrane device [11,12].

Effective mixing is of major importance in many fields in chemical engineering [13]. The conversion and selectivity of chemical reactions in the liquid phase might heavily depend upon mixing. Mixing devices and processes can be characterized by the use of competitive (either consecutive or parallel) reaction schemes. There are two main examples: the azo dye stuff coupling of 1-naphtol and 2-naphtol with diazotized sulfanilic acid [14], and the iodide–iodate reaction scheme [15–17]. Both systems were originally developed for the characterization of stirred tanks.

In this study, the iodide–iodate reaction was used as a test reaction to investigate reactive mixing in a hollow fiber device both theoretically and experimentally. The iodide–iodate method is based on a competitive parallel reactions system [15]:

$$H_2BO_3^- + H^+ \leftrightarrow H_3BO_3 \quad \text{(i)}$$

$$5I^- + IO_3^- + 6H^+ \leftrightarrow 3I_2 + 3H_2O \quad \text{(ii)}$$

The reaction of iodate and iodide to iodine (also named the "Dushman reaction") (ii) is fast, but is much slower than the neutralization of dihydroborate ions (i). The iodine I_2 formed can further react with iodide ions I^- to yield I_3^- ions according to the quasi-instantaneous equilibrium:

$$I^- + I_2 \leftrightarrow I_3^- \quad \text{(iii)}$$

The I_3^- concentration is then measured by spectrophotometry at 353 nm.

The method is based on adding in stoichiometric defect a small quantity of sulphuric acid to a mixture of iodate, iodide and borate ions [17]. In perfect mixing conditions, the injected acid is instantaneously dispersed in the reactive medium and consumed by borate ions according to the neutralization reaction (i) which is infinitely

* Corresponding author at: LAGEP, Université de Lyon, UMR 5007, CNRS, CPE, 43 bd du 11 novembre, 69100 Villeurbanne, France. Tel.: +33 4 72 43 18 67; fax: +33 4 72 43 16 99.
E-mail address: charcosset@lagep.univ-lyon1.fr (C. Charcosset).

1385-8947/$ – see front matter © 2008 Elsevier B.V. All rights reserved.
doi:10.1016/j.cej.2008.12.020

Nomenclature

A	light absorption (–)
$[i]^0$	initial concentration of reactant i (mol/m^3)
D_i	diffusion coefficient of reactant i (m^2/s)
K_B	equilibrium constant of reaction (iii) (l/mol)
k_j	kinetic constant for reaction j (–)
l	optical path length (m)
L	length of the hollow fiber (m)
$\mathbf{N}_i$	molecular flux of reactant i (mol/m^2 s)
$N_{i,in}$	total molecular flux of reactant i calculated at the inlets (mol/s)
$Q_{in,L}$	flow rate at the inlet of the lumen side (m^3/s)
$Q_{in,S}$	flow rate at the inlet of the shell side (m^3/s)
$Q_{out,L}$	flow rate at the outlet of the lumen side (m^3/s)
r	radial coordinate (m)
R	inner radius of the hollow fiber (m)
r_j	reaction rate of reaction j (mol/m^3 s)
R_i	specific rate of formation of reactant i (mol/m^3 s)
t	time (s)
$\boldsymbol{v}$	velocity vector (m/s)
v	norm of the velocity vector (m/s)
$v_{in,L}$	maximum velocity at the inlet of the lumen side (m/s)
$v_{in,S}$	velocity at the inlet of the shell side (m/s)
X_S	segregation index (–)
z	axial coordinate (m)
Greek letters	
ε	molar extinction coefficient (m^2/mol)
ρ	fluid density (kg/m^3)
η	dynamic viscosity (Pa s)

faster than reaction (ii). In the opposite situation, when the characteristic dissipation time of the acid aggregates (micromixing time) is in the same range or larger than the characteristic reaction time of reaction (ii), these aggregates involve a local over concentration of acid which after complete consumption of $H_2BO_3^-$ reacts with iodide and iodate surrounding ions to yield iodine. The selectivity of iodine is then a measure of the segregation state of the fluid. Therefore, borate ions have a twofold role. They are reactants of the neutralization reaction (i), and they play the role of buffer to keep constant the pH of the solution. This pH value is judiciously chosen owing to the potential-pH diagram of the water–iodine system [17].

If micromixing is perfect, the acid is totally and instantaneously neutralized by the first reaction, and iodine does not appear. Conversely, if micromixing is slow, a local excess of acid induces iodine formation, yielding I_3^-. The segregation index may be calculated as follows [15–16]:

$$X_S = \frac{Y}{Y_{ST}} \tag{1}$$

where Y is the ratio of the acid mole number consumed by the slow reaction (the creation of iodine I_2 and I_3^-) and the total acid mole number:

$$Y = 2\frac{n_{I_2} + n_{I_3^-}}{n_{H^{+0}}} \tag{2}$$

Finally, Y_{ST} is the value of Y in a total segregation case when mixing is considered to be infinitely slow. With this, the two reactions appear as quasi-instantaneous compared to mixing and acid is consumed in proportion to the local concentration of both borate and iodide/iodate ions. Y_{ST} is then related to the concentration of the formed iodine:

$$Y_{ST} = \frac{6[IO_3^-]^0}{6[IO_3^-]^0 + [H_2BO_3^-]^0} \tag{3}$$

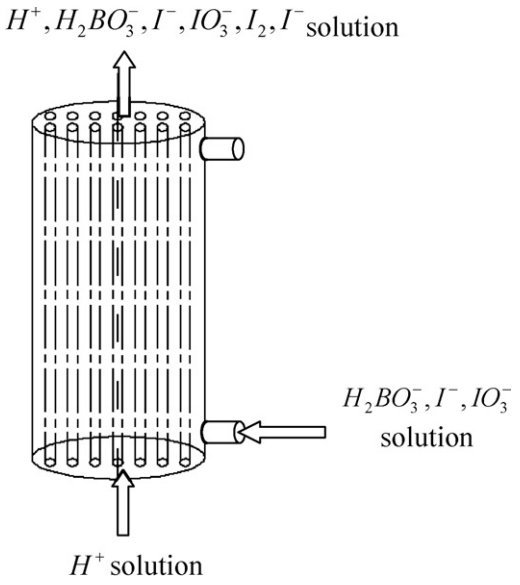

Fig. 1. Representative view of the iodide–iodate reaction in a hollow fiber membrane device.

A small value of X_S denotes a good mixing process since a low segregation index indicates either fast mixing or homogeneous mixing or a combination of both. Therefore, X_S is equal to zero for perfect micromixing and to one for a totally segregated medium. The iodide–iodate reaction scheme has been applied to the characterization of various mixing devices, such as stirred tanks [15–17], Taylor-Couette reactors [18], and microstructured mixing devices [13,19–21]. Panić et al. [21] proposed initial concentrations for the chemicals, suitable to characterize microstructured mixer devices in order to obtain maximum sensitivity of the method and a final pH of the resulting mixture that produces stable iodine concentrations.

This paper presents numerical simulations and experimental data of the iodide–iodate method in a hollow fiber device (Fig. 1). Numerical simulations predicted the profile of the various species and the segregation index at the outlet of the lumen side of a hollow fiber. The experimental measurements of the segregation index were carried out under various experimental conditions and for two different hollow fiber devices. Both theoretical and experimental studies aim to contribute to a better qualitative understanding of reactive mixing in a hollow fiber membrane device. In the lumen side of the hollow fiber, mixing is obtained by diffusion of the various species in the laminar flow; therefore the term "micromixing" (mixing at the molecular level) may also apply. However, this term does not refer exactly to the phenomena occurring during mixing at the molecular level in a stirred tank in a turbulent flow.

2. Theory

Fig. 2 shows a hollow fiber of length L and radius R (2D geometry) in a cylindrical coordinate system. The complete 3D geometry can be obtained from the 2D geometry under the hypothesis of axial symmetry. The sulphuric acid is introduced at the inlet of the lumen side. The mixture of iodate, iodide and borate ions flows from the inlet of the shell side.

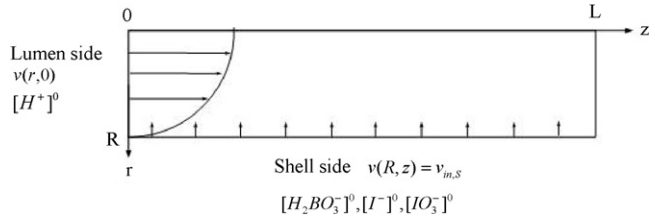

Fig. 2. Representative view of the lumen side of a hollow fiber (axial symmetry). The $[H^+]$ solution enters from the lumen side and the $[H_2BO_3^-]$, $[IO_3^-]$ and $[I^-]$ solution from the shell side of the hollow fiber.

The inlet velocity at the lumen side, $v_{in,L}$, is the maximum velocity of the parabolic profile. The inlet velocity at the shell side, $v_{in,S}$, is assumed to be uniform along the membrane length and equal to the flow rate at the shell side, $Q_{in,S}$, divided by the membrane surface $2\pi RL$ (for one fiber). This assumption implies that the porosity of the membrane surface is rather high, which is verified for membranes used for such applications. It also implies that the pressure drop from the inlet to the outlet on the lumen side is relatively low compared to the pressure applied on the shell side. This assumption is verified for the cases investigated. If this was not the case, the whole hollow fiber has to be taken into account (lumen side + porous membrane) for the simulation of the velocity profile [22].

In laminar flow, the Navier–Stokes equations apply:

$$\rho\frac{\partial v}{\partial t} - \eta\Delta v + \rho(v\cdot\nabla)v + \nabla p = \mathbf{0}$$
$$\nabla\cdot\mathbf{v} = 0 \quad (4)$$

where $\mathbf{v}$, p, ρ and η denote respectively the velocity vector, the pressure, the density of the fluid and the dynamic viscosity. In the following, the norm of the velocity vector, $\mathbf{v}$, will be noted v. The density and the viscosity data are those of water ($\rho = 1\times10^3$ kg/m^3 and $\eta = 1\times10^{-3}$ Pa s).

Mixing is obtained by diffusion of the various species in the lumen side of the hollow fiber. The transfer equations are the convection–diffusion equations with a reaction term:

$$\frac{\partial C_i}{\partial t} + \nabla\cdot(-D_i\nabla C_i + C_i\mathbf{v}) = R_i$$
$$i = H^+,\ H_2BO_3^-,\ I^-,\ IO_3^-,\ I_2,\ I_3^- \quad (5)$$

with C_i, D_i, R_i respectively the concentration, diffusion coefficient and specific rate of formation of reactant i.

The specific rates of formation are obtained from the reaction rates. The kinetics of reaction (i) may be written as [23]:

$$r_1 = k_1[H^+][H_2BO_3^-] \quad \text{with } k_1 = 10^8\ \text{m}^3/\text{mol s at } 25\,^\circ\text{C} \quad (6)$$

For reaction (ii), the kinetics has been experimentally determined and can be expressed as [24]:

$$r_2 = k[IO_3^-][I^-]^2[H^+]^2 \quad \text{with } k_2 = 4.27\times10^{-4}\ \text{m}^{12}/\text{mol}^4\,\text{s at } 25\,^\circ\text{C} \quad (7)$$

Finally, the kinetics of reaction (iii) can be expressed as [24]:

$$r_3 = k_3[I^-][I_2] - k_3'[I_3^-] \quad \text{with } k_3 = 5.9\times10^6\ \text{m}^3/\text{mol s and } k_3' = 7.5\times10^6/\text{s at } 25\,^\circ\text{C} \quad (8)$$

The initial concentration, diffusion coefficient and specific rate of formation of each reactant are specified in Table 1.

The boundary conditions are expressed as follows (Table 2). At the inlet of the lumen side, the flow is assumed to be fully developed and a parabolic profile for the axial velocity, v_z, is specified, with $v_{in,L}$ being the maximum velocity. At the inlet of the shell side, the radial velocity, v_r, is set to $-v_{in,S}$. At the outlet of the lumen side, the relative pressure is set to zero (the solution flows at atmospheric pressure).

The molecular fluxes of the introduced components are specified at the inlet of the lumen and shell sides. At $r = 0$, axial symmetry conditions are specified.

The software COMSOL Multiphysics™ (Grenoble, France) is used to solve the differential equations set, by the finite element method and the direct linear system solvers UMFPACK and SPOOLES.

3. Materials and methods

3.1. Materials

KIO_3 and H_3BO_3 powders were obtained from Sigma–Aldrich, and KI from VWR. NaOH was provided by Ridel-deHaën and the sulphuric acid solution by Fluka.

Two hollow fiber membrane devices were tested. The MiniKros hollow fiber device was provided by Spectrum (CellD, Roquemaure, France). This device contained 545 polyethylenesulfone fibers (PES) with an inner radius of 250×10^{-6} m. The hollow fiber MiniModule 1×5.5 device was provided by Liqui-Cel (Alternative Marketing, Hoerdt, France). The device contained 2300 polypropylene fibers

Table 1
Characteristic values of the iodide–iodate reaction in a hollow fibers device.

Species	Diffusion coefficient (m^2/s)	Initial Concentration (mol/m^3)	Specific rate of formation (mol/m^3 s)
H^+	9.311×10^{-9} [25]	$[H^+]^0 = 10$ or 30	$-k_1[H^+][H_2BO_3^-] - 6k_2[H^+]^2[IO_3^-][I^-]^2$
$H_2BO_3^-$	1×10^{-9} [26]	$[H_2BO_3^-]^0 = 89.8$ [21]	$-k_1[H^+][H_2BO_3^-]$
IO_3^-	1.078×10^{-9} [25]	$[IO_3^-]^0 = 6.35$ [21]	$-k_2[H^+]^2[IO_3^-][I^-]^2$
I^-	2.045×10^{-9} [25]	$[I^-]^0 = 31.9$ [21]	$-5k_2[H]^2[IO_3^-][I^-]^2 - k_3[I^-][I_2] + k_3'[I_3^-]$
I_2	1.36×10^{-9} [27]	$[I_2]^0 = 0$	$3k_2[H]^2[IO_3^-][I^-]^2 - k_3[I^-][I_2] + k_3'[I_3^-]$
I_3^-	1×10^{-9} [28]	$[I_3^-]^0 = 0$	$k_3[I^-][I_2] - k_3'[I_3^-]$

Table 2
Boundary conditions for the numerical simulation of velocity and concentration profiles in the lumen side of a hollow fiber.

Position	v_r	v_z	Specie flux
$z = 0$	$v_r = 0$	$v_z = v_{in,L}\left[1-\left(\frac{r}{R}\right)^2\right]$	$-\mathbf{n}.\mathbf{N}_{H^+} = [H^+]^0 v_{in,L}$
$r = R$	$v_r = -v_{in,S}$	$v_z = 0$	$-\mathbf{n}.\mathbf{N}_i = [i]^0 v_{in,S}$ $\quad i = H_2BO_3^-,\ I^-,\ IO_3^-$

Table 3
Characteristics of the hollow fiber membrane devices.

Device	Number of fibers	Pore size (μm)	Fiber inner radius (μm)	Fiber length (m)	Area (m^2)
MiniKros	545	0.2	250	0.208	0.18
Minimodule	2300	0.03	110	0.115	0.18

with an inner radius of 110×10^{-6} m. The overall characteristics of these two devices are summarized in Table 3: number of fibers, mean pores size, inner radius of the hollow fibers (R), length of the hollow fibers (L), and surface area.

3.2. Experimental set-up

The experimental set-up is shown in Fig. 3. It included a pump (Sartorius), a hollow fiber device, a manometer placed at the inlet of the lumen side. At the inlet of the hollow fiber device, a tank contained the H^+ solution. The pressurized vessel (Millipore) contained the mixture of iodate, iodide and borate ions. It was equipped with a manometer and connected to the nitrogen bottle and to the hollow fiber device on the shell side.

3.3. Solutions preparation

3.3.1. Sulphuric acid solution

The acid solution (2 l) was prepared with a commercial concentrated solution to have $[H^+] = 10$ *or* 30×10^{-3} mol/l.

3.3.2. Iodide, iodate, borate solution

KI and KIO_3 powders were first dissolved in separate solutions. H_3BO_3 and NaOH were then mixed to obtain the buffer solution to which are added KI and KIO_3 solutions and water. This sequence of mixing operation must be carefully followed so that iodide and iodate ions coexist in a basic solution which prevents thermodynamic iodine formation.

The iodide, iodate (stoichiometric mixture) and borate ions solution contained the following concentrations:

$$[I^-]^0 = 31.9 \times 10^{-3} \text{ mol/l}$$
$$[IO_3^-]^0 = 6.35 \times 10^{-3} \text{ mol/l} \Rightarrow [I_2]_{\text{potential}} = 3[IO_3^-]^0 = 3/5[I^-]^0 \approx 19.05 \times 10^{-3} \text{ mol/l}$$
$$[H_3BO_3]^0 = 17.96 \times 10^{-2} \text{ mol/l and } [NaOH]^0 = 89.8 \times 10^{-3} \text{ mol/l}$$
$$\Rightarrow [H_2BO_3^-] = [H_3BO_3] = 89.8 \times 10^{-3} \text{ mol/l (Buffer solution : pH} = pKa_1 = 9.14)$$

As a strong base, soda totally reacted with orthoboric acid to form an equimolecular mixture $H_2BO_3^-/H_3BO_3$. The pH of the buffer was then equal to $pKa_1 = 9.14$, which corresponds to the first acidity of the orthoboric acid [15].

To prepare 2 l of solution, the following amounts of reactants were then required:

$m_{KI} = 10.5884$ g dissolved in 20 ml water,
$m_{KIO_3} = 2.7217$ g dissolved in 200 ml water,
$m_{H_3BO_3} = 22.209$ g dissolved in 800 ml water,
$m_{NaOH} = 7.249$ g dissolved in 200 ml water.

3.4. Experimental protocol

The iodate, iodide and borate solution was placed in the pressurized vessel, and the H^+ solution in the inlet tank. At time $t = 0$, the reactants were mixed by opening the valve. The flowrates entering the inlet of the lumen and shell sides, $Q_{in,L}$ and $Q_{in,S}$, respectively, were measured. The velocities at the inlet of the lumen and shell sides are calculated by dividing the flowrates data by the respective area: $v_{in,L} = 2Q_{in,L}/N\pi R^2$, $v_{in,S} = Q_{in,S}/2N\pi RL$. At the end of the experiment, the hollow fibers device was rinsed with 2 l pure water.

3.5. Iodine concentration measurements by spectrophotometry

According to the Beer–Lambert law, the light absorption A is proportional to the I_3^- concentration through the molar extinction coefficient ε of I_3^- at 353 nm.

$$[I_3^-] = \frac{A}{\varepsilon \ell} \text{ (mol/m}^3\text{)} \quad (9)$$

where l is the optical path length. ε has been determined equal to 2127 m^2/mol.

3.6. Determination of the segregation index X_S

In order to quantify the mixing quality, the results are expressed by the segregation index X_S, whose values lie between 0 and 1:

Perfect micromixing : $X_S = 0$

Total segregation : $X_S = 1$

Partial segregation : $X_S = \dfrac{Y}{Y_{ST}}$

with:

$$Y = 2\frac{n_{I_2} + n_{I_3^-}}{n_{H^{+0}}} = 2\frac{Q_{out,L}[I_2]_{out,L} + Q_{out,L}[I_3^-]_{out,L}}{Q_{in,L}[H^+]^0} \quad (10)$$

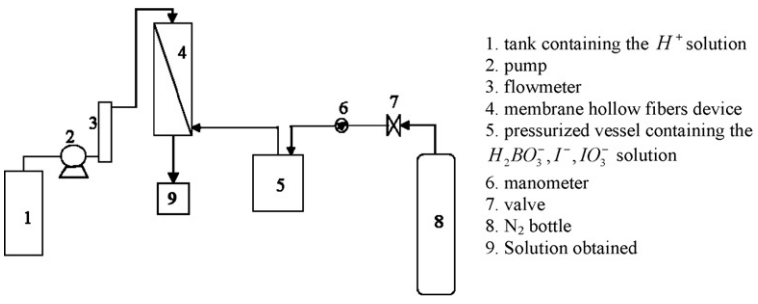

Fig. 3. Experimental set-up for the iodide–iodate reaction in a hollow fibers device.

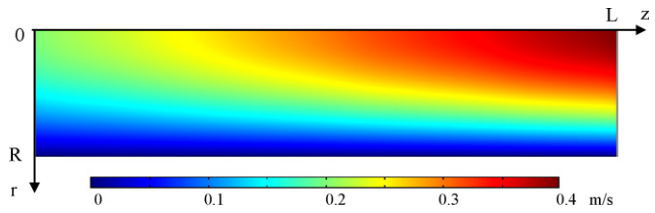

Fig. 4. Velocity profile in the lumen side of a hollow fiber $v_{in,L} = 0.2$ m/s; $v_{in,S} = 5 \times 10^{-5}$ m/s.

Mass balances on iodine atoms yield the following expressions:

$$[I^-] = [I^-]_0 - \frac{5}{3}([I_2] + [I_3^-]) - [I_3^-] \quad (11)$$

$$[I_3^-] = K_B[I_2][I^-] \quad (12)$$

where K_B is the equilibrium constant of reaction (iii).

By combining these two equations, we obtain a second-order algebraic equation of the iodine concentration:

$$-\frac{5}{3}[I_2]^2 + \left[[I^-]^0 - \frac{8}{3}[I_3^-]\right][I_2] - \frac{[I_3^-]}{K_B} = 0 \quad (13)$$

The equilibrium constant K_B is a function of temperature T [29]:

$$\log_{10} K_B = \frac{555}{T} + 7.355 - 2.575 \log_{10} T \quad K_B \text{ in l/mol} \quad (14)$$

at 25 °C K_B = 702 l/mol.

4. Results

4.1. Velocity profile

Fig. 4 represents the velocity profile in the lumen side of the hollow fiber for the following parameters $v_{in,L} = 0.2$ m/s and $v_{in,S} = 5 \times 10^{-5}$ m/s. In this case, the two flowrates entering the device at the inlet of the lumen side and inlet of the shell side were the same. The velocity profile was almost parabolic along the fiber length with a maximum velocity increasing continuously due to the fluid permeation [11]. It was verified that at the outlet of the lumen side the maximum velocity $v_{max} = 0.398$ m/s $\approx 2v_{in,L}$, which was explained by the flow balance at the outlet of the lumen side.

4.2. Concentration profiles

All the following results were obtained at steady state ($t > t_R = L/v_{in,L}$). Fig. 5a–f show the concentration profiles of the various species at time t = 2 s. The results were obtained for the following parameters: $[H^+]^0 = 10$ mol/m^3, $v_{in,L} = 0.2$ m/s and $v_{in,S} = 1.25 \times 10^{-5}$ m/s. The hollow fiber length was L = 0.1 m and the inner radius $R = 1 \times 10^{-4}$ m. For $v_{in,L} = 0.2$ m/s, the residence time, t_R, between the inlet and the outlet of the lumen side was t_p = 1.15 s. Therefore, the concentration profiles were well established at time t = 2 s.

The H^+ ions were introduced at the inlet of the lumen side (Fig. 5a) and the $H_2BO_3^-$, I^-, IO_3^- ions at the inlet of the shell side (Fig. 5b–d). The ions were consumed progressively in the "mixing zone" of the hollow fiber. This mixing zone was defined previously as the part of the hollow fiber where both **A** and **B** reactants were both present [11]. Mixing was here obtained by diffusion of the various species. Near the inlet of the lumen side, the $H_2BO_3^-$ ions were consumed by the H^+ ions. The I^- and IO_3^- ions reacted also in the mixing zone. However, they did not participate to the H^+ consumption as early as $H_2BO_3^-$, as the redox reaction (ii) was fast, but was much slower than the neutralization reaction (i).

I_2 and I_3^- were produced near the inlet of the hollow fiber, with a maximum concentration respectively equal to 0.0115 and 0.045 mol/m^3 (Fig. 5e and f). For the simulation of $BaSO_4$ precipitation, we previously reported high supersaturation data in this part of the lumen side of the hollow fiber [6–7]. This result confirms that this part of the hollow fiber will be easily fouled by growing particles.

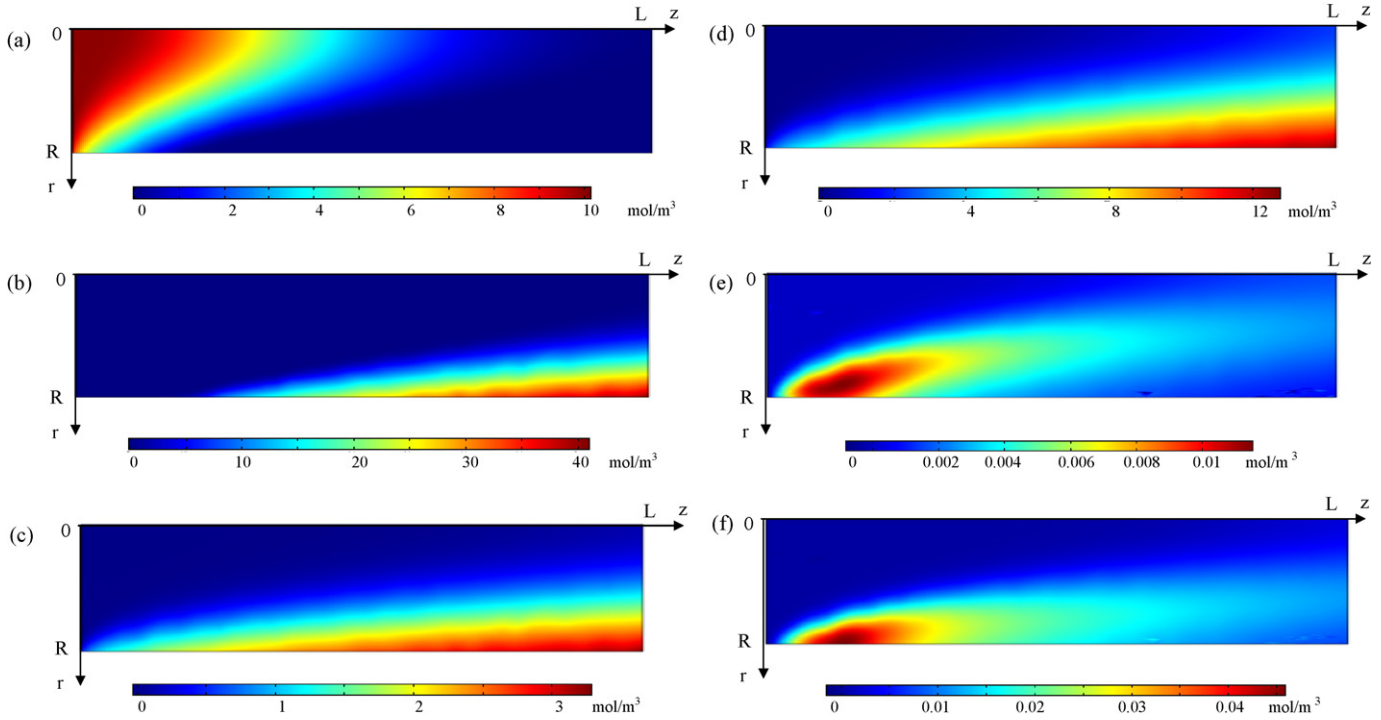

Fig. 5. Concentration profiles of the various species in the lumen side of a hollow fiber for the following parameters: $[H^+]^0 = 10$ mol/m^3, $v_{in,L} = 0.2$ m/s and $v_{in,S} = 1.25 \times 10^{-5}$ m/s; (a) $[H^+]$; (b) $[H_2BO_3^-]$; (c) $[IO_3^-]$; (d) $[I^-]$; (e) $[I_2]$; and (f) $[I_3^-]$.

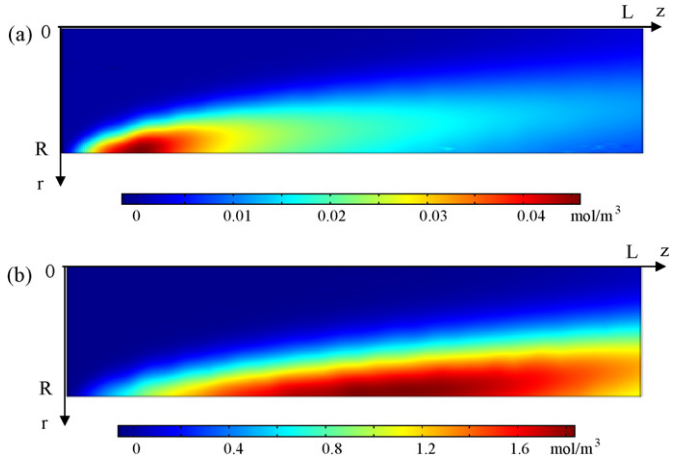

Fig. 6. Influence of the initial concentration $[H^+]^0$ on the $[I_3^-]$ concentration profile in the lumen side of a hollow fiber for the following parameters: $v_{in,L} = 0.2$ m/s and $v_{in,S} = 1.25 \times 10^{-5}$ m/s; (a) $[H^+]^0 = 10$ mol/m^3, and (b) $[H^+]^0 = 30$ mol/m^3.

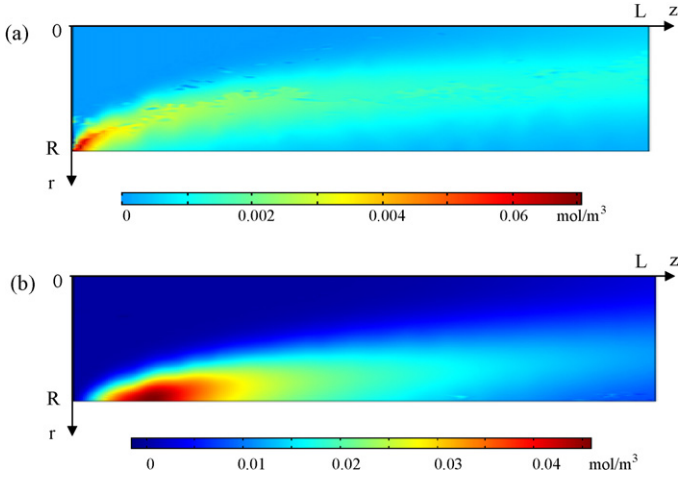

Fig. 7. Influence of the inlet flow velocity on the $[I_3^-]$ concentration profile in the lumen side of a hollow fiber for the following parameters: $[H^+]^0 = 10$ mol/m^3 and $v_{in,L} = 0.2$ m/s; (a) $v_{in,S} = 5 \times 10^{-5}$ m/s, and (b) $v_{in,S} = 1.25 \times 10^{-5}$ m/s.

4.3. Influence of the inlet concentration $[H^+]^0$ on the $[I_3^-]$ profile

The influence of the inlet concentration $[H^+]^0$ on the $[I_3^-]$ profile in the lumen side of the hollow fiber is shown in Fig. 6a and b. The results were obtained for the following parameters: $v_{in,L} = 0.2$ m/s, $v_{in,S} = 1.25 \times 10^{-5}$ m/s, $[H^+]^0 = 10$ mol/m^3 and $[H^+]^0 = 30$ mol/m^3. $[H^+]^0$ has a major impact on the I_3^- profile. For $[H^+]^0 = 10$ mol/m^3, I_3^- ions were found only in a small part of the lumen side of the fiber and the maximum concentration of $[I_3^-]$ was equal to 0.045 mol/m^3. For $[H^+]^0 = 30$ mol/m^3, I_3^- ions were produced in a much larger part of the fiber, the maximum concentration was higher and equal to 1.6 mol/m^3. The relation of the maximum concentration of $[I_3^-]$ to $[H^+]^0$ was non-linear. This may be explained by the excess of H^+, as the $H_2BO_3^-$ ions were totally consumed. In the following, the introduced concentration $[H^+]^0$ was set to 10 mol/m^3.

4.4. Influence of the inlet velocity at the shell side on the $[I_3^-]$ profile

Fig. 7a and b show the influence of the inlet velocity at the shell side $v_{in,S}$ on the $[I_3^-]$ profile in the lumen side of the hollow fiber. The results are obtained for the following parameters: $[H^+]^0 = 10$ mol/m^3, $v_{in,L} = 0.2$ m/s, $v_{in,S} = 1.25 \times 10^{-5}$ m/s and $v_{in,S} = 5 \times 10^{-5}$ m/s. For $v_{in,S} = 5 \times 10^{-5}$ m/s, I_3^- ions were found in a small part of the fiber and the maximum I_3^- concentration was equal to 7×10^{-3} mol/m^3. For $v_{in,S} = 1.25 \times 10^{-5}$ m/s, I_3^- was produced in a larger part of the fiber, the maximum concentration was higher and equal to 0.045 mol/m^3. Although the amount of reactants $H_2BO_3^-$, I^-, IO_3^- introduced was then 4 times higher for $v_{in,S} = 5 \times 10^{-5}$ m/s, the amount of I_3^- produced was lower. This was explained by effective mixing obtained at higher velocities. In most of the simulations, the inlet velocity at the shell side, $v_{in,S}$, was set to $v_{in,S} = 1.25 \times 10^{-5}$ m/s.

4.5. Segregation index obtained from the numerical simulations

The segregation index Y_{ST} was obtained from the numerical simulations as follows:

$$X_S = \frac{Y}{Y_{ST}} \tag{15}$$

$$Y = 2\frac{\int\int_{z=L}[I_2](r,z)v dS + \int\int_{z=L}[I_3^-](r,z)v(r,z)dS}{[H^+]^0 \pi R^2 v_{max}/2} \tag{16}$$

$$Y_{ST} = \frac{6[IO_3^-]^0}{6[IO_3^-]^0 + [H_2BO_3^-]^0} \tag{17}$$

where the integrations were computed at the outlet of the lumen side of the fiber ($z = L$). The data were obtained at time $t = 2$ s (Table 4).

For the same inlet velocities, the segregation index increased with an increasing acid concentration (from $[H^+]^0 = 10$ mol/m^3 to $[H^+]^0 = 30$ mol/m^3). This was in accordance with the $[I_3^-]$ profiles. This phenomenon was also observed in stirred tanks [15], and was explained as follows. The acid reacts in both reactions. If there is a decrease of acid concentration the rates of the protonation reaction (i) and of the Dushman reaction (ii) are slowed down. The rate of the reaction (ii) is more sensitive to acid concentration than the rate of (i) because its order with respect to acid is higher. So if we decrease the acid concentration, we increase the difference between the two reaction rates. The Dushman reaction becomes slower, less iodine is produced and X_S decreases.

For high velocity entering the lumen side and $[H^+]^0 = 10$ mol/m^3 the segregation index kept low indicating that mixing was effective. However, for the same conditions and $[H^+]^0 = 30$ mol/m^3, the segregation index was much higher. This was due to the excess in H^+ ions in the lumen side of the hollow fiber. Therefore, with the mixed solution: $[I^-]^0 = 31.9$ mol/m^3, $[IO_3^-]^0 = 6.35$ mol/m^3 and $[H_2BO_3^-]^0 = 89.8$ mol/m^3, the H^+ concentration was set to 10 mol/m^3.

Table 4
Segregation indexes obtained from the numerical simulations.

(mol/m^3) $[H^+]^0$	$v_{in,L}$(m/s)	$v_{in,S}$(m/s)	$\int\int_{z=L}[I_2]v dS$	$\int\int_{z=L}[I_3^-]v dS$	X_s
10	0.2	5×10^{-5}	3.22×10^{-13}	5.15×10^{-12}	1.17×10^{-3}
10	0.2	1.25×10^{-5}	7.76×10^{-12}	3.57×10^{-11}	9.30×10^{-3}
30	0.2	1.25×10^{-5}	9.26×10^{-10}	2.94×10^{-9}	0.276

Table 5
Segregation indexes obtained from the experimental results.

Device	$[H^+]^0$ (mol/m^3)	$Q_{in,S} = Q_{in,L}$ (ml/s)	A	$[I_3^-]$ (mol/m^3)	$[I_2]$ (mol/m^3)	X_s
Minimodule	10	3	0.310	1.45×10^{-2}	6.51×10^{-4}	2.05×10^{-2}
Minimodule	10	5	0.185	8.58×10^{-3}	3.83×10^{-6}	1.15×10^{-2}
Minimodule	10	7	0.070	3.31×10^{-3}	1.47×10^{-4}	4.424×10^{-3}
MiniKros	10	3	0.803	4.10×10^{-2}	1.82×10^{-3}	5.75×10^{-2}

4.6. Segregation indexes obtained from the experiments

The segregation index was measured experimentally at the outlet of the two hollow fibers device for $[H^+]^0 = 10\,mol/m^3$ and various inlet flowrates (the inlet flowrates at the lumen and shell sides were equal). The segregation index was found between 4.24×10^{-3} and 5.75×10^{-2}, indicating effective mixing (Table 5). Moreover, the segregation index decreased with an increasing flowrate. This phenomenon was previously observed for mixing in micromixers [19] and in a hollow fiber device [12]. It confirms that mixing in hollow fibers device is more effective at higher flowrates. Moreover, the obtained segregation index was lower with the MiniModule ($X_S = 2.05 \times 10^{-2}$) than with the MiniKros device ($X_S = 5.75 \times 10^{-2}$), for the same inlet flowrates. This also confirms that lower hollow fiber radius favours mixing [11].

From the experimental data obtained with the Minimodule at $Q_{in,S} = Q_{in,L} = 7\,ml/s$ ($v_{in,L} = 0.16\,m/s$ and $v_{in,S} = 3.8 \times 10^{-5}\,m/s$), a comparison can be made with the segregation index obtained numerically for similar velocities: $v_{in,L} = 0.2\,m/s$ and $v_{in,S} = 5 \times 10^{-5}\,m/s$, and the same inlet concentrations: $[H^+]^0$, $[I^-]^0$, $[IO_3^-]^0$ and $[H_2BO_3^-]^0$. The experimental segregation index was equal to 4.24×10^{-3}, and the segregation index obtained from the numerical simulation was equal to 1.17×10^{-3}. This identical range of data suggests that our numerical simulations are accurate.

The comparison between theoretical and experimental data was not performed exactly for the same velocity data. The reason is that instabilities appeared in the simulations at smaller velocities ($< v_{in,L} = 0.2\,m/s$), and that the experiences could not be realized at higher flowrates ($> v_{in,L} = 0.16\,m/s$). Moreover, the numerical results relied on a number of approximations, i.e. (i) approximation for the diffusion coefficient for the species $H_2BO_3^-$ and I_3^-, (ii) the rate of the Dushman reaction was taken independent on the ionic strength (the dependence on the ionic strength would imply local data for the reaction rate, and therefore would increase considerably the time for the simulations), (iii) the reaction kinetics of the Dushman reaction is not fully known. It was pointed out recently that comparison of published models of the Dushman reaction showed large differences due to the complexity of the iodine-forming reaction under various reagent concentrations and ionic strength conditions [23]. Qualitatively the iodide–iodate method provides reliable results for assessing the extent of micromixing of miscible reagents, however further study of the Dushman reaction are needed to reach quantitative treatment. Another dataset on the kinetics would influence the concentration profiles obtained from the simulations, and therefore the segregation index. The experimental measurements relied also on a number of approximations, i.e. (i) the segregation index was measured at the outlet of the hollow fiber device and not directly at the outlet of a single fiber, (ii) the measurement was not realized instantaneously. As a consequence, a comparison between the range of data obtained for the experimental and theoretical segregation indexes may be more appropriate than an exact comparison.

5. Conclusions

Qualitatively the iodide–iodate method, in which the iodine yield is measured, has provided reliable results for assessing the extent of micromixing of miscible reagents [23]. This study aims to provide a qualitative understanding of reactive mixing in a hollow fiber membrane device. By using the iodide–iodate method, we studied numerically and experimentally reactive mixing in a hollow fiber device. The segregation index, X_S, was found in the range 10^{-2}–10^{-3}, for appropriate reactant concentrations, indicating effective mixing. For comparison, the segregation index in a stirred vessel achieves values of 0.1–0.3 depending on the feed point [15]. Mixing processes in microchannels give a segregation index between 10^{-2} and 10^{-3}, but a direct comparison of the different devices is difficult, due to the various mixing effects. These results confirm that hollow fiber membrane devices may be used as micromixer devices. The numerical simulations showed that I_3^- ions were produced mainly in the first part of the lumen side of the hollow fiber. This confirmed our previous results on precipitation where high supersaturation data and experimental fouling were obtained in this part of the hollow fibers [6].

References

[1] K.K. Sirkar, P.V. Shanbhag, A.S. Kovvali, Membrane in a reactor: a functional perspective, Ind. Eng. Chem. Res. 38 (1999) 3715–3737.
[2] E. Drioli, A. Criscuoli, E. Curcio, Membrane contactors and catalytic membrane reactors in process intensification, Chem. Eng. Technol. 26 (2003) 975–981.
[3] Z. Jia, Z. Liu, Synthesis of nanosized $BaSO_4$ particles with a membrane reactor: effects of operating parameters, J. Membr. Sci. 209 (2002) 153–161.
[4] Z. Jia, Z. Liu, F. He, Synthesis of nanosized $BaSO_4$ and $CaCO_3$ particles with a membrane reactor: effects of additives on particles, J. Colloid Interface Sci. 66 (2003) 322–327.
[5] G.G. Chen, G.S. Luo, J.H. Xu, J.D. Wang, Membrane dispersion precipitation method to prepare nanoparticles, Powder Technol. 139 (2004) 180–185.
[6] R. Kieffer, D. Mangin, F. Puel, C. Charcosset, Precipitation of barium sulphate in a hollow fiber membrane contactor: Part I. Investigation of particulate fouling, Chem. Eng. Sci. (2009), in press.
[7] R. Kieffer, D. Mangin, F. Puel, C. Charcosset, Precipitation of barium sulphate in a hollow fiber membrane contactor: Part II. The influence of process parameters, Chem. Eng. Sci. (2009), in press.
[8] H. Fei, Z. Jia, P. Yuelian, Z. Liu, Synthesis of polyaluminium chloride with a membrane reactor: effects of operating modes, J. Membr. Sci. 227 (2003) 15–21.
[9] D.M. Zarkadas, K.K. Sirkar, Antisolvent crystallization in porous hollow fiber devices, Chem. Eng. Sci. 61 (2006) 5030–5048.
[10] C. Charcosset, H. Fessi, Preparation of nanoparticles with a membrane contactor, J. Membr. Sci. 266 (2005) 115–120.
[11] R. Kieffer, C. Charcosset, F. Puel, D. Mangin, Numerical simulation of mass transfer in a liquid–liquid membrane contactor for laminar flow conditions, Comput. Chem. Eng. 32 (2008) 1333–1341.
[12] Z. Jia, Y. Zhao, L. Liu, F. He, Z. Liu, A membrane reactor intensifying micromixing: effects of parameters on segregation index, J. Membr. Sci. 276 (2006) 295–300.
[13] A. Kölbl, M. Kraut, K. Schubert, The iodide iodate method to characterize microstructured mixing devices, AIChE J. 54 (2008) 639–645.
[14] J.R. Bourne, O.M. Kut, J. Lenzner, An improved system to investigate micromixing in high-intensity mixers, Ind. Eng. Chem. Res. 31 (1992) 949–958.
[15] M.C. Fournier, L. Falk, J. Villermaux, A new parallel competing reaction system for assessing micromixing efficiency—experimental approach, Chem. Eng. Sci. 51 (1996) 5053–5064.
[16] M.C. Fournier, L. Falk, J. Villermaux, A new parallel competing reaction system for assessing micromixing efficiency—determination of micromixing time by a simple mixing model, Chem. Eng. Sci. 51 (1996) 5187–5192.
[17] P. Guichardon, L. Falk, Characterisation of micromixing efficiency by the iodide–iodate reaction system. Part I. Experimental procedure, Chem. Eng. Sci. 55 (2000) 4233–4243.
[18] D.L. Marchisio, A.A. Barresi, CFD simulation of mixing and reaction: the relevance of the micro-mixing model, Chem. Eng. Sci. 58 (2003) 3579–3587.
[19] N. Kockmann, T. Kiefer, M. Engler, P. Woias, Convective mixing and chemical reactions in microchannels with high flow rates, Sens. Actuators B 117 (2006) 495–508.

[20] H. Monnier, A.M. Wilhelm, H. Delmas, Effects of ultrasound on micromixing in flow cell, Chem. Eng. Sci. 55 (2000) 4009–4020.
[21] S. Paníc, S. Loebbecke, T. Tuercke, J. Antes, D. Bošković, Experimental approaches to a better understanding of mixing performance of microfluidic devices, Chem. Eng. J. 101 (2004) 409–419.
[22] R. Kieffer, F. Puel, D. Mangin, C. Charcosset, Simulation of velocity and concentration profiles in a hollow fiber membrane contactor for reactive mixing, submitted for publication.
[23] J.R. Bourne, Comments on the iodide/iodate method for characterising micromixing, Chem. Eng. J. 140 (2008) 638–641.
[24] P. Guichardon, L. Falk, J. Villermaux, Characterisation of micromixing efficiency by the iodide–iodate reaction system: Part II. Kinetic study, Chem. Eng. Sci. 55 (2000) 4245–4253.
[25] D.R. Lide (Ed.), Handbook of Chemistry and Physics, CRC Press, Cleveland, OS, USA, 2003.
[26] H.G. Linge, Anodic oxidation of pyrrhotite in simulated cip liquors, Miner. Eng. 8 (1995) 795–806.
[27] L. Cantrel, R. Chaouche, J. Chopin-Dumas, Diffusion coefficients of molecular iodine in aqueous solutions, J. Chem. Eng. Data 42 (1997) 216–220.
[28] A.G. Kontos, M. Fardis, M.I. Prodromidis, T. Stergiopoulos, E. Chatzivasiloglou, G. Papavassiliou, P. Falaras, Morphology, ionic diffusion and applicability of novel polymer gel electrolytes with LiI/I_2, Phys. Chem. Chem. Phys. 8 (2006) 767–776.
[29] D.A. Palmer, R.W. Ramette, R.E. Mesmer, Triodide ion formation equilibrium and activity coefficients in aqueous solution, J. Solution Chem. 13 (1984) 673–683.